A pixel-based likelihood framework for analysis of fluorescence recovery after photobleaching data

J.K. JONASSON*, N. LORÉN†, P. OLOFSSON‡, M. NYDÉN§
& M. RUDEMO**

Mathematical Sciences, Chalmers University of Technology and Gothenburg University, Göteborg, Sweden

†*Structure and Material Design, SIK, The Swedish Institute for Food and Biotechnology, Göteborg, Sweden*

‡*Structure and Material Design, SIK, The Swedish Institute for Food and Biotechnology, Göteborg, Sweden*

§*Department of Chemical and Biological Engineering, Chalmers University of Technology, Göteborg, Sweden*

**Mathematical Sciences, Chalmers University of Technology and Gothenburg University, Göteborg, Sweden*

Summary

A new framework for the estimation of diffusion coefficients from data on fluorescence recovery after photobleaching (FRAP) with confocal laser scanning microscopy (CLSM) is presented. It is a pixel-based statistical methodology that efficiently utilizes all information about the diffusion process in the available set of images. The likelihood function for a series of images is maximized which gives both an estimate of the diffusion coefficient and a corresponding error. This framework opens up possibilities (1) to obtain localized diffusion coefficient estimates in both homogeneous and heterogeneous materials, (2) to account for time differences between the registrations at the pixels within each image, and (3) to plan experiments optimized with respect to the number of replications, the number of bleached regions for each replicate, pixel size, the number of pixels, the number of images in each series etc. To demonstrate the use of the new framework, we have applied it to a simple system with polyethylene glycol (PEG) and water where we find good agreement with diffusion coefficient estimates from NMR diffusometry. In this experiment, it is also shown that the effect of the point spread function is negligible, and we find fluorochrome-concentration levels that give a linear response function for the fluorescence intensity.

Correspondence to: J.K. Jonasson. Tel: +46(0)31-7725317; fax: +46(0)31-161973; e-mail: jenny@chalmers.se

Introduction

Mass transport in supramolecular biomaterials is of crucial importance for many industrial applications such as controlled release of drugs in pharmaceuticals, release of flavour, aroma and vitamins in foods, protein purification, water management in hygiene products and swelling properties of hydrogels. Molecular mass transport is determined by the interaction between the transported molecules and the surrounding microstructure in which the molecules are transported (Hermansson *et al.*, 2006) and also the interaction between the transported molecules themselves. Several mass transport mechanisms exist depending on the length scales present in the material and the properties of the diffusing molecules. Here the focus will be on molecular self-diffusion.

There exist many methods to determine the molecular diffusion rate (Westrin *et al.*, 1994). One of the most frequently used methods is nuclear magnetic resonance diffusometry (NMRd). With NMRd it is possible to determine the diffusion rate with high accuracy in many types of materials non-invasively. However, the interpretation of the NMRd results in complex systems regarding the actual diffusion mechanism is not trivial. Previous work has shown that it is beneficial to combine NMRd with different microscopy techniques and modelling in order to separate between structural and interaction mechanisms (Lorén *et al.*, 2005; Walther *et al.*, 2006). Many industrially important systems such as emulsions, gels and phase-separated polymer mixtures are heterogeneous at the micrometre scale. In these systems, the local diffusion properties most probably vary with the position

due to heterogeneity, and the global diffusion properties will be a result of some kind of averaging of the local diffusion properties. To be able to understand the relationship between the diffusion properties and the structure of heterogeneous systems, it would therefore be highly useful to be able to simultaneously determine, in a spatially resolved manner, the diffusion rate and the structure.

Fluorescence recovery after photobleaching (FRAP) offers possibilities to determine the local diffusion rate and the surrounding structure simultaneously. In FRAP, the diffusion rate of fluorescent molecules is determined locally directly in the microscope. The fluorescent molecules are deactivated or bleached in a limited volume through a short high intensity laser pulse. This results in a local decrease of the fluorescence in the bleached volume. After the bleaching, or more precisely immediately after the start of the bleaching, adjacent unbleached fluorochromes diffuse into the bleached volume and vice versa, resulting in a broadening of the bleached volume and a recovery of the fluorescence intensity inside it. The rate of recovery is proportional to the local molecular diffusion rate, which makes it possible to quantitatively determine diffusion coefficients. For reviews of the FRAP method and its application to different materials and research areas, see (Meyvis et al., 1999; Lippincott-Schwartz et al., 2001; Phair & Misteli, 2001; Weiss, 2004; Sprague & McNally, 2005).

The first FRAP experiments and FRAP data evaluation models were mainly based on the use of nonscanning fluorescence microscopes (Axelrod et al., 1976; Soumpasis, 1983; Tsay & Jacobson, 1991; Berk et al., 1993). These models described the relation between the diffusion in a bleached two-dimensional region and the fluorescence recovery. Confocal laser scanning microscopy (CLSM) is a fluorescence-based microscopy technique in which the images emerge from a thin optical section in the material (Pawley, 2006). Arbitrary regions can be bleached in the CLSM, making it an excellent equipment with which to perform FRAP experiments, and the combination CLSM-FRAP is a versatile technique to simultaneously determine a spatially dependent diffusion rate and the corresponding structure directly in the microscope. To determine local diffusion properties, CLSM-FRAP has been used in different applications with structures such as cells, membranes, gels and solutions (Smedt et al., 1997; Burke et al., 2000; Cheng & Prud'homme, 2002; Verkman, 2003; Sonesson et al., 2005; Chen et al., 2006; Perry et al., 2006; Alvarez-Mancenido et al., 2006).

For use with CLSM, only a few FRAP models exist (Braeckmans et al., 2003). A first practical but approximate three-dimensional model that uses a stationary laser beam for bleaching and a line-scanning beam for recording the fluorescence recovery was developed in 1993 (Blonk et al., 1993). Then, two- and three-dimensional models for high numerical aperture objectives, fast line-scanning, multiphoton, and diffusion during bleaching have been developed (Kubitscheck et al., 1994; Wedekind et al., 1994, 1996; Kubitscheck et al., 1998; Brown et al., 1999; Siggia et al., 2000; Braga et al., 2004). Recently, a FRAP model considering line-wise bleaching of arbitrary regions (Braeckmans et al., 2003) and a fast complementary line FRAP model (Braeckmans et al., 2007) have been developed. Up to now, most FRAP models determine the diffusion rate from the time-dependent variation of the average intensity of the bleached region. Attempts to develop models that take the time-dependent evolution of the entire concentration profile have been made (Keuren & Schrof, 2003; Seiffert & Oppermann, 2005). However, existing methods typically do not contain any model for the measurement noise and do not include standard errors for the obtained diffusion coefficient estimates.

In this paper, the diffusion rate will be estimated from a pixel-based statistical model for the time-dependent changes of the pixel intensities. A likelihood function is computed for all observed pixel values in a series of consecutive images. This likelihood function can be numerically optimized, which gives both an estimate of the diffusion coefficient and the corresponding standard error. The effect of the detection point spread function is included in the model and the effect of it is analysed by the use of simulations. To demonstrate the use of the new model, an experiment with polyethylene glycol was performed, in which the diffusion coefficient was estimated and compared with corresponding NMR diffusometry measurements. We discuss computational details and find regions with proportionality between fluorescence intensity and fluorochrome concentration, which is a requirement for unbiased diffusion coefficient estimation. In the concluding discussion, we describe how the suggested methodology can be used to design optimal CLSM-FRAP experiments.

Theory

Model

The pixels in the images will be modelled individually, combining a solution to the diffusion equation and statistical likelihood theory (Pawitan, 2001). The diffusion of flourochromes is supposed to follow the usual diffusion equation (Crank, 1975)

$$\frac{\partial C}{\partial t} = D \left(\frac{\partial^2 C}{\partial x^2} + \frac{\partial^2 C}{\partial y^2} + \frac{\partial^2 C}{\partial z^2} \right), \qquad (1)$$

where C is the concentration of unbleached fluorochromes and D is the diffusion coefficient. Regard a rotationally symmetric bleached region and assume that there is no net diffusion in the z-direction and that the fluorescent molecules are initially uniformly distributed. Using polar coordinates, the diffusion equation can be written

$$\frac{\partial C}{\partial t} = D \left(\frac{1}{r} \frac{\partial C}{\partial r} + \frac{\partial^2 C}{\partial r^2} \right), \qquad (2)$$

where r is the distance from the centre of the bleached region. Let $C_0(r)$ denote the concentration function at time zero, and let $I_0(x) = (1/\pi) \int_0^\pi \exp(-x \cos t) dt$ denote the modified Bessel function of order zero. Then the solution of Eq. (2) can be written on the form

$$C(r, t) = \frac{1}{2Dt} \exp\left(-\frac{r^2}{4Dt}\right)$$
$$\times \int_0^\infty u C_0(u) I_0\left(\frac{ru}{2Dt}\right) \exp\left(-\frac{u^2}{4Dt}\right) du. \quad (3)$$

Immediately after the bleaching the concentration profile is approximately described by an inverse top hat function. However, after the bleaching, the diffusion starts to blur this profile and an approximately Gaussian concentration profile develops. Let us therefore assume an initial concentration of the form

$$C_0(r) = a_0 - \frac{a_1}{r_0^2} \exp\left(-\frac{r^2}{r_0^2}\right), \quad (4)$$

an assumption which will be studied in the result section below. Then the solution in Eq. (3) simplifies to

$$C(r, t) = a_0 - \frac{a_1}{4Dt + r_0^2} \exp\left(-\frac{r^2}{4Dt + r_0^2}\right). \quad (5)$$

If the concentration of fluorochromes is low enough, the fluorescence is proportional to the concentration. Hence, the pixel value, $p(i, t)$, at pixel i at distance r_i from the centre of the bleached region at time t is proportional to the concentration $C(r_i, t)$. The noise in the images is assumed to be independent between pixels and in time and, in addition, normally distributed with mean zero and constant variance σ^2. Hence the pixel value $p(i, t)$ is normally distributed with mean $C(r_i, t)$ and variance σ^2, and its probability density is

$$f\left(p(i, t); a_0, a_1, D, r_0, \sigma^2\right) = \frac{1}{\sqrt{2\pi\sigma^2}}$$
$$\times \exp\left(-\frac{(p(i, t) - C(r_i, t))^2}{2\sigma^2}\right).$$

The likelihood function is defined as the joint probability distribution function for all pixels at all times and due to the independence it is

$$L\left(a_0, a_1, D, r_0, \sigma^2\right) = \prod_{t\in T} \prod_{i\in S} f\left(p(i, t); a_0, a_1, D, r_0, \sigma^2\right)$$
$$= \prod_{t\in T} \prod_{i\in S} \frac{1}{\sqrt{2\pi\sigma^2}}$$
$$\times \exp\left(-\frac{(p(i, t) - C(r_i, t))^2}{2\sigma^2}\right),$$

where T is the set of times and S is the set of pixels. The likelihood, or rather the log-likelihood,

$$l(\theta) = \log L(\theta) = -\frac{|T||S|}{2} \log\left(2\pi\sigma^2\right)$$
$$-\frac{1}{2\sigma^2} \sum_{t\in T} \sum_{i\in S} (p(i, t) - C(r_i, t))^2, \quad (6)$$

is maximized with respect to the parameter vector $\theta = (a_0, a_1, D, r_0, \sigma^2)$ to find the most likely parameter values, the ml estimates, given the observed images. Likelihood theory allows straightforward computation of error estimates of the parameters. For large samples the parameter estimates are approximately multivariate normally distributed with a covariance matrix that can be approximated with the inverse of the observed information matrix. The entry in row j and column k of the observed information matrix is

$$-\frac{\partial^2}{\partial\theta_j\theta_k} l(\theta),$$

evaluated at $\theta = \hat{\theta}$, where $\hat{\theta}$ is the ml estimate of θ. If the coordinates of the centre of the bleached disk are unknown, there will be two extra parameters in the likelihood.

Fluorescence intensity and fluorochrome concentration

The analysis of FRAP data relies on the assumption that the fluorescence intensity is approximately linearly proportional to the concentration of fluorochromes. This relation is only valid if the concentration of fluorescent molecules is sufficiently small. Otherwise photons may be subject to quenching by multiple absorptions and emissions, an effect called inner filtering (van Oostveldt & Bauwens, 1990). Generally the fluorescence intensity F is given (Herman, 1998) by the equation $F = QI_0(1 - e^{-A})$, where I_0 is the light intensity, Q is the quantum yield of the fluorochrome, and A is the absorbance. The amount of light absorbed by the fluorochromes is proportional to the concentration of flourochromes, and we can replace A with kc, a constant times the concentration c, and obtain the equation

$$F = QI_0(1 - e^{-kc}). \quad (7)$$

When c is small, $1 - e^{-kc} \approx kc$. Thus for small concentrations we have approximately

$$F = QI_0 kc. \quad (8)$$

The detection point spread function

Following Braeckmans *et al.*, (2003) we assume that the detection point spread function is of the form

$$I_d(x, y, z) = I_{0d} \exp\left(-2\frac{x^2 + y^2}{r_r^2}\right) \exp\left(-2\frac{z^2}{r_z^2}\right),$$

where I_{od} is a constant, r_r is the resolution in the x and y directions and r_z is the resolution in the z direction. The detected fluorescence in a point (x, y, z) at time t is then

$$F(x, y, z, t) = \int_{-\infty}^\infty \int_{-\infty}^\infty \int_{-\infty}^\infty I_d(x', y', z')$$
$$\times C(x - x', y - y', z - z', t) dx' dy' dz'.$$

Using Eq. (5) we get with polar coordinates

$$F(r,t) = I_{0d} r_z r_r^2 \left(\frac{\pi}{2}\right)^{3/2} \left(a_0 - \frac{a_1}{4Dt + r_0^2 + r_r^2/2}\right.$$
$$\left. \times \exp\left\{-\frac{r^2}{4Dt + r_0^2} \cdot \frac{8Dt + 2r_0^2 + 2r_r^2}{8Dt + 2r_0^2 + r_r^2}\right\}\right).$$

(9)

Equation (5) or (9) is then used in Eq. (6) to estimate the parameter vector θ. If the resolution in the x and y direction is small compared to the radius of the bleached disk the effect of the detection point spread function on the measured diffusion is negligible and Eq. (5) can be used instead of Eq. (9).

Materials and methods

Materials

The polyethylene glycol used, with an average molecular weight (M_r) of 3000 Da, was made by Fluka. Deuterium oxide with a purity of 99.8% was provided by ARMAR Chemicals, Switzerland. The fluorescent probe, made by Fluka, was Sodium Fluorescein with a molecular weight of 376.28 Da.

Sample preparation

A solution containing 20 (w/w%) polyethylene glycol, sodium fluorescein and deuterium oxide was made. The polyethylene glycol was mixed with sodium fluorescein and deuterium oxide and dissolved during gentle stirring over night at room temperature. All solutions containing sodium fluorescein were covered by aluminium foil in order to avoid bleaching of the solution in advance. The solution was then analysed using CLSM-FRAP and NMR diffusometry.

Confocal laser scanning microscopy

The CLSM system used consists of a Leica SP2 AOBS (Heidelberg, Germany). The solution was poured into a small metallic cup with a diameter of approximately 15 mm and a depth of 2 mm which was sealed with a cover glass. The solution was analysed at room temperature (21°C) with the CLSM. A water immersion objective with 20× magnification and a numerical aperture of 0.5 was used with water as immersion medium. The pinhole was set to one Airy unit and no beam expander was used resulting in a smaller effective numerical aperture. The emission maximum at 488 nm of a 75 mW Argon laser was used in the FRAP experiments and wavelengths between 510 nm and 590 nm were detected. The laser intensity before the AOTF (Acusto optical tunable filter) was set to approximately 60% of full power. The FRAP protocol was as follows. First, 25 pre-bleach images were recorded with the AOTF set to 2%. Then, the bleaching was performed once, i.e. only one bleach-image was recorded. The AOTF was set to

100% during the bleaching. In addition, the zoom-in-function was used to increase the efficiency of the bleaching in order to fulfil the condition that the distance between adjacent lines during bleaching is less than half of the spatial resolution (Braeckmans *et al.*, 2003). Finally, 100 images were recorded during the post-bleaching with the AOTF set to 2%. All FRAP series were recorded at a position 30 micrometres under the surface of the sample. The size of the bleached region was 30 micrometres and always placed in the centre of the image. The small numerical aperture of the objective and the large bleached region result in a cylindrical bleaching geometry. Four well-separated positions in the solution were analysed with FRAP. The FRAP images were stored as 12-bit tif-images. The size of the images was chosen so that the intensity of the corners in the images should not be influenced with more than around 1% reduction in intensity by the bleaching. An image size of 187.5 micrometres and a zoom factor four were used in this work. Two different combinations of image format and scan rate were used to determine the effect of pixel size and the number of information carrying pixels on the diffusion coefficient estimate. The image format and the scan rate were combined so that the pixel dwell time was constant. In the first combination, an image format of 128×128 pixels and a scan rate of 800 Hz were used, leading to an image acquisition time of 0.34 s. In the second combination, an image format of 256×256 pixels and a scan rate of 400 Hz were used, leading to an image acquisition time of 0.99 s.

In practise, based on the assumptions made in the present model the following conditions should be met in the CLSM-FRAP experiment:

- Initially, the fluorescent molecules are uniformly distributed
- An isotropic diffusion process takes place in a medium considered to have infinite size
- There is no flow in the medium
- Objectives have a low numerical aperture
- At the first post-bleach image the concentration profile is approximately Gaussian

The last assumption is specific to the algorithm used in the present paper, but not to the likelihood approach in general. The assumption is discussed in the concluding section of the paper.

NMR diffusometry

The NMRd experiments were performed on a Varian Unity Inova 500 MHz spectrometer equipped with a dedicated diffusion probe supplied by DOTY Sci. USA. The probe provides 4.8 T/m at 10 A current. The stimulated echo pulse sequence was used in all experiments and the gradient pulse length was 4 ms. Sine-shaped gradients were used to minimize eddy current effects. The maximum gradient strength was varied so that at least a ten-fold decrease in signal intensity was obtained at the highest gradient strength used for each

diffusion experiment. The diffusion constant was estimated by a standard nonlinear least square fitting procedure in Matlab. The corresponding standard deviation was obtained by a Monte Carlo approach in which the fitting procedure was repeated 500 times with random signal intensities as calculated from the deviation between the previous fit and the raw data.

Partial derivatives of the log likelihood

Computation of the partial derivatives of the log likelihood in Eq. (6) with respect to the parameters improves the optimization. The partial derivatives are

$$\frac{\partial l}{\partial \sigma^2} = -\frac{|T||S|}{2\sigma^2} + \frac{1}{2\sigma^4} \sum_{t \in T} \sum_{i \in S} (p(i,t) - C(r_i,t))^2,$$

and

$$\frac{\partial l}{\partial \theta_j} = \frac{1}{\sigma^2} \sum_{t \in T} \sum_{i \in S} (p(i,t) - C(r_i,t)) \frac{\partial C(r_i,t)}{\partial \theta_j}$$

for $\theta_j = a_0, a_1, D, r_0$. The partial derivatives of C in Eq. (5) are straightforward to compute. For instance, we find

$$\frac{\partial C(r_i,t)}{\partial D} = \frac{4a_1 t}{(4Dt + r_0^2)^2} \exp\left\{ -\frac{r_i^2}{4Dt + r_0^2} \right\} \left(1 - \frac{r_i^2}{4Dt + r_0^2}\right).$$

Starting point for the likelihood maximization

To find a good starting point for the maximization of Eq. (6), we can fit the model for one image at one time point. Put

$$C(r) = b_0 - b_1 \exp\left(-b_2 r^2\right) \tag{10}$$

and maximize the log-likelihood

$$l(b_0, b_1, b_2, \sigma^2) = -\frac{|S|}{2} \log\left(2\pi\sigma^2\right)$$
$$- \frac{1}{2\sigma^2} \sum_{i \in S} (p(i) - C(r_i))^2. \tag{11}$$

Note that if we have estimates of b_0, b_1 and b_2 in Eq. (10) we get corresponding estimates of a_0, a_1 and $4Dt + r_o^2$ in Eq. (5).

The derivatives of the log likelihood in Eq. (11) with respect to the parameters are,

$$\frac{\partial l}{\partial b_0} = \frac{1}{\sigma^2} \sum_{i \in S} \left\{ p(i) - b_0 + b_1 \exp\left(-b_2 r_i^2\right) \right\},$$

$$\frac{\partial l}{\partial b_1} = -\frac{1}{\sigma^2} \sum_{i \in S} \left\{ p(i) - b_0 + b_1 \exp\left(-b_2 r_i^2\right) \right\} \exp\left(-b_2 r_i^2\right),$$

$$\frac{\partial l}{\partial b_2} = \frac{1}{\sigma^2} \sum_{i \in S} \left\{ p(i) - b_0 + b_1 \exp\left(-b_2 r_i^2\right) \right\} b_1 r_i^2 \exp\left(-b_2 r_i^2\right),$$

$$\frac{\partial l}{\partial \sigma^2} = -\frac{|S|}{2\sigma^2} + \frac{1}{2\sigma^4} \sum_{i \in S} (p(i) - C(r_i))^2.$$

Setting these partial derivatives equal to 0, we get the following equations for the mL parameter estimates,

$$\hat{\sigma}^2 = \frac{1}{|S|} \sum_{i \in S} (p(i) - C(r_i))^2,$$

$$\hat{b}_0 = \frac{1}{|S|} \sum_{i \in S} p(i) + \hat{b}_1 \frac{1}{|S|} \sum_{i \in S} \exp\left(-\hat{b}_2 r_i^2\right),$$

$$\hat{b}_1 = \frac{\frac{1}{|S|} \sum_{i \in S} p(i) \exp\left(-\hat{b}_2 r_i^2\right) - \left(\frac{1}{|S|} \sum_{i \in S} p(i)\right)\left(\frac{1}{|S|} \sum_{i \in S} \exp\left(-\hat{b}_2 r_i^2\right)\right)}{\left(\frac{1}{|S|} \sum_{i \in S} \exp\left(-\hat{b}_2 r_i^2\right)\right)^2 - \frac{1}{|S|} \sum_{i \in S} \exp\left(-2\hat{b}_2 r_i^2\right)}.$$

The estimate $\hat{b}_2$ is obtained by solving the equation

$$\frac{1}{|S|} \sum_{i \in S} p(i) r_i^2 \exp\left(-\hat{b}_2 r_i^2\right) - \left(\frac{1}{|S|} \sum_{i \in S} p(i)\right)$$
$$\times \left(\frac{1}{|S|} \sum_{i \in S} r_i^2 \exp\left(-\hat{b}_2 r_i^2\right)\right) + \left\{\frac{1}{|S|} \sum_{i \in S} p(i) \exp\left(-\hat{b}_2 r_i^2\right)\right.$$
$$\left. - \left(\frac{1}{|S|} \sum_{i \in S} p(i)\right)\left(\frac{1}{|S|} \sum_{i \in S} \exp\left(-\hat{b}_2 r_i^2\right)\right)\right\} \times$$
$$\left\{\frac{1}{|S|} \sum_{i \in S} r_i^2 \exp\left(-2\hat{b}_2 r_i^2\right) - \left(\frac{1}{|S|} \sum_{i \in S} \exp\left(-\hat{b}_2 r_i^2\right)\right)\right.$$
$$\left. \times \left(\frac{1}{|S|} \sum_{i \in S} r_i^2 \exp\left(-\hat{b}_2 r_i^2\right)\right)\right\} \Big/$$
$$\left\{\left(\frac{1}{|S|} \sum_{i \in S} \exp\left(-\hat{b}_2 r_i^2\right)\right)^2 - \frac{1}{|S|} \sum_{i \in S} \exp\left(-2\hat{b}_2 r_i^2\right)\right\} = 0$$

for $\hat{b}_2$.

Computational details

Before the analysis the background is subtracted from the images. A sequence of 25 pre-bleach images is obtained. An average background image is created as a pixel-wise average of all these pre-bleach images. The background is then subtracted from all the post-bleach images. To get the same order of magnitude in the pixel levels as before the subtraction, the average over all pixels in the averaged background is added to the post-bleach images.

To maximize the log-likelihood in Eq. (6) it is essential to have a good initial guess of the parameter values. To achieve this we look at the likelihood for single images with known, or otherwise determined, centre coordinates, which makes it possible to solve for all but one of the parameter values analytically as described in the previous section. Analysis of the first two bleach images gives estimates of all parameters. These parameter values are then used as initial guesses when maximizing the total likelihood. The computations are performed in MATLAB 7.3.0 using the optimization routine fminunc. Partial derivatives of the likelihood function are used in the optimization. Calculation of initial guesses of the parameters and the maximization of the total likelihood takes about 20 s for 48 images of size 128×128 pixels and about 30 s for 18 images of size 256×256 pixels using a laptop with 2.0 GHz processor and 2 GB RAM. The MATLAB program is available upon request to the corresponding author.

If the centre coordinates are unknown they could in principle be estimated using the total likelihood. When necessary we have instead used only the first image to estimate the centre coordinates and then diagnostic plots, see the Result section below, can easily determine whether or not the bleached area or the sample has moved.

Results

Fluorescence intensity and fluorochrome concentration

Experiments were performed to study the relationship between fluorescence intensity and fluorochrome concentration with solutions of PEG and deuterium oxide. All experimental conditions except the fluorochrome concentration were held constant in the two experiments. In the upper part of Fig. 1 we show results from an experiment with high fluorochrome concentrations and a corresponding fit of Eq. (7). We see that the equation with the exponential curve gives a good fit and that we are well out of the domain of linearity between fluorescence intensity and fluorochrome concentration. Conversely, the lower part of Fig. 1 shows results from an experiment with low fluorochrome concentrations and a corresponding fit of Eq. (8). Here we see that the equation with the linear response curve gives a good fit and that we are well within of the domain of linearity between the two variables. Therefore, based on these results, a fluorochrome concentration of 25 ppm was chosen for the subsequent FRAP experiments.

Effect of the detection point spread function

The experimental resolution should theoretically be $r_r = 0.61\lambda_{em}/NA$, where λ_{em} is the emission wavelength and NA is the numerical aperture, which in our case gives $r_r = 0.622\,\mu m$. The relation $r_r = 0.61\lambda_{em}/NA$ is valid for conventional fluorescence microscopy. But for CLSM,
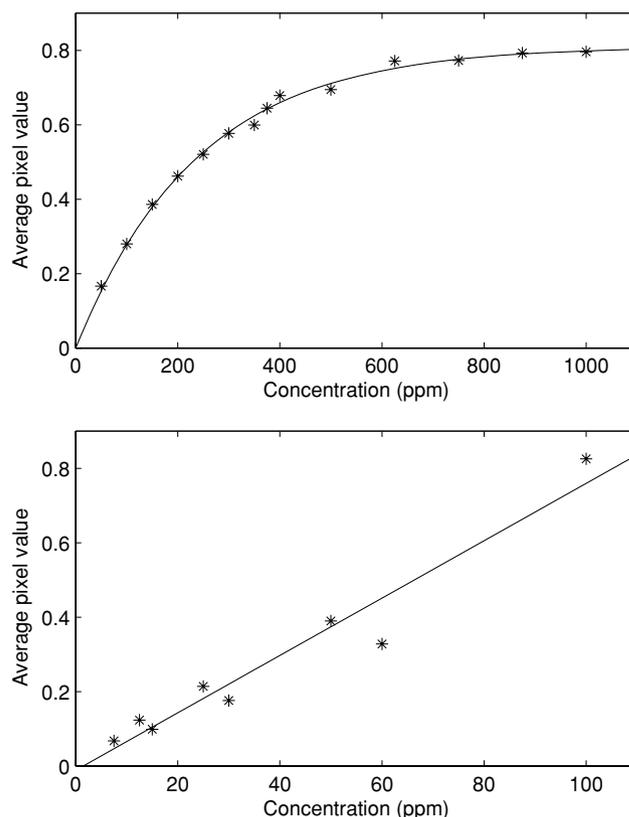
Fig. 1. Relationship between fluorescence intensity and fluorochrome concentration in two series of experiments. The upper graph shows results from a series with high fluorochrome concentrations and a corresponding fit of the exponential response curve in Eq. (7), and the lower graph shows results from an experiment with low fluorochrome concentrations and a corresponding fit of the linear response curve in Eq. (8).

the spatial resolution is approximately 30% better than in conventional fluorescence microscopy (Diaspro, 2002). On the other hand, the effective spatial resolution in the present experiments was somewhat worse than indicated by the formula since no beam expander was used.

The effect of the detection point spread function will be negligible if the spatial resolution r_r is small enough. To see how small it needs to be simulations have been made using Eqs (5) and (9) with different values of the resolution. The noise is independent and normally distributed with variance σ^2 as described above. The parameters are estimated with the log-likelihood in Eq. (6), e.g. the resolution is not estimated. The true parameter values and the average diffusion coefficient $\hat{D}$ estimated from 500 simulations are shown in Table 1. The random number generator was reset to the same seed before each simulation series. The diffusion coefficients are calculated from 18 images with pixel size 0.732 μm/pixel, 256×256 pixels per image and 0.995 s between the images. In the simulations, resolutions of $r_r = 0.622\,\mu m$ times an integer were used. It is seen in Table 1 that the result of the point spread function is a decrease of the diffusion coefficient

Table 1. Results from simulations with different resolutions, when the point spread function is not used in the estimation of the diffusion coefficient. The values of the parameters are $a_0 = 0.7$, $a_1 = 160.75 \, \mu m^2$, $D = 64.300 \, \mu m^2/s$, $r_0 = 26.39 \, \mu m$ and $\sigma = 0.0548$.

$r_r \, (\mu m)$	$\hat{D} \, (\mu m^2/s)$	$s \, (\mu m^2/s)$
-	64.389	0.586
0.622	64.358	0.595
1.244	64.206	0.586
2.489	63.670	0.597
4.978	61.561	0.610

estimate, and the influence of the point spread function is increasing with increasing resolution r_r.

In particular, the simulation results show that in this work the spatial resolution r_r is sufficiently small and the bleaching area is sufficiently large for the effect of the detection point spread function to be negligible. Hence, to simplify the estimation of the diffusion coefficient the formula without the detection point spread function will be used hereafter.

Diffusion in PEG solutions

To demonstrate the use of the framework developed in this work, we have applied our model and FRAP experiments to a solution of PEG and deuterium oxide. This solution was used because it is easy to alter the viscosity without changing the solubility conditions. However, here the aim was to demonstrate the likelihood FRAP framework and not to study the effect of viscosity on diffusion rate and, therefore, only one solution was prepared. The results of the estimation of the diffusion coefficients and the associated standard deviations from the likelihood are shown in Table 2. The standard deviation in column 4 in the table refers to the standard deviation computed via the likelihood method. The average and standard deviation in columns 5 and 6 are the average and standard deviation of the four replicates, i.e. the four measurement positions.

Table 2. Results from estimation of diffusion coefficients. For the first four estimates 48 images were used and for the last four images 18 images were used.

Replicate	No pixels	$D \, (\mu m^2/s)$	$s \, (\mu m^2/s)$	$\bar{D} \, (\mu m^2/s)$	$s_{repl} \, (\mu m^2/s)$
1	128×128	64.3	0.8		
2	128×128	60.1	0.8		
3	128×128	61.1	0.8		
4	128×128	59.6	0.8	61.3	2.1
1	256×256	61.0	0.5		
2	256×256	61.8	0.5		
3	256×256	60.8	0.4		
4	256×256	63.8	0.5	61.8	1.4

An example of analysed images and the fit to the concentration function are shown in Figs 2 and 3. As the images are noisy it is hard to see the fit plotting the pixel values of all pixels versus the distance from the centre of the bleached disk. Instead the averages of pixels within annuli, centred at the bleached region, with the same width are calculated. These averages are plotted versus the centres of their annuli together with the estimated function in Eq. (5).

The results from the NMRd measurements were $D = 62.0 \, \mu m^2/s$ with a standard deviation of $1.9 \, \mu m^2/s$.

Discussion, conclusions and outlook

The diffusion coefficient estimated using the likelihood approach agrees well with the NMRd measurements and the error estimates are rather small. It can be seen that the error estimates are smaller for the 256×256 pixels images than for the 128×128 pixels images. The fit of the model is also good judging from the diagnostic plots, Fig. 3, with the possible exception of a minor deviation in the first image. This is not surprising because of the chosen initial concentration function. Using another initial concentration function, we could in principle solve the integral in Eq. (3) numerically. In combination with the likelihood optimization this seems too time consuming, but alternative methods are currently being developed, see below. Note, however, that already in the second image in Fig. 3 obtained after 1 s the fit with a Gaussian profile is good (except for the first noisy point based on very few pixels).

The images were not compensated for drift in the laser signal, since the observed drift was small and compensation for it did not improve the results. Similarly, use of more images in the analysis only caused marginal changes in the diffusion coefficient estimates and the error estimate did not decrease. This pinpoints the stability of the suggested likelihood-based framework.

Comparing with other methods the likelihood FRAP analysis has the advantage of using the data more effectively since every pixel value is used individually. As this framework leads to more precise evaluation it requires less laser intensity during bleaching and thus decreases the risk of photo damage of sensitive structures. Moreover, it is straightforward to compute standard errors of the diffusion coefficient estimates. Methods that utilize the average intensity in the bleached region have estimates that are sensitive to the specification of the right size of the bleached region. That is not the case with the likelihood FRAP analysis, since the size of the bleached region is a parameter in the model which is estimated.

The main aim of this paper is to show the advantages of using the likelihood approach in the FRAP modelling and analysis. Several improvements can, however, be made, for instance regarding the concentration modelling and the description of the error distribution. The noise is probably better described by a Poisson distribution since the detector counts photons.
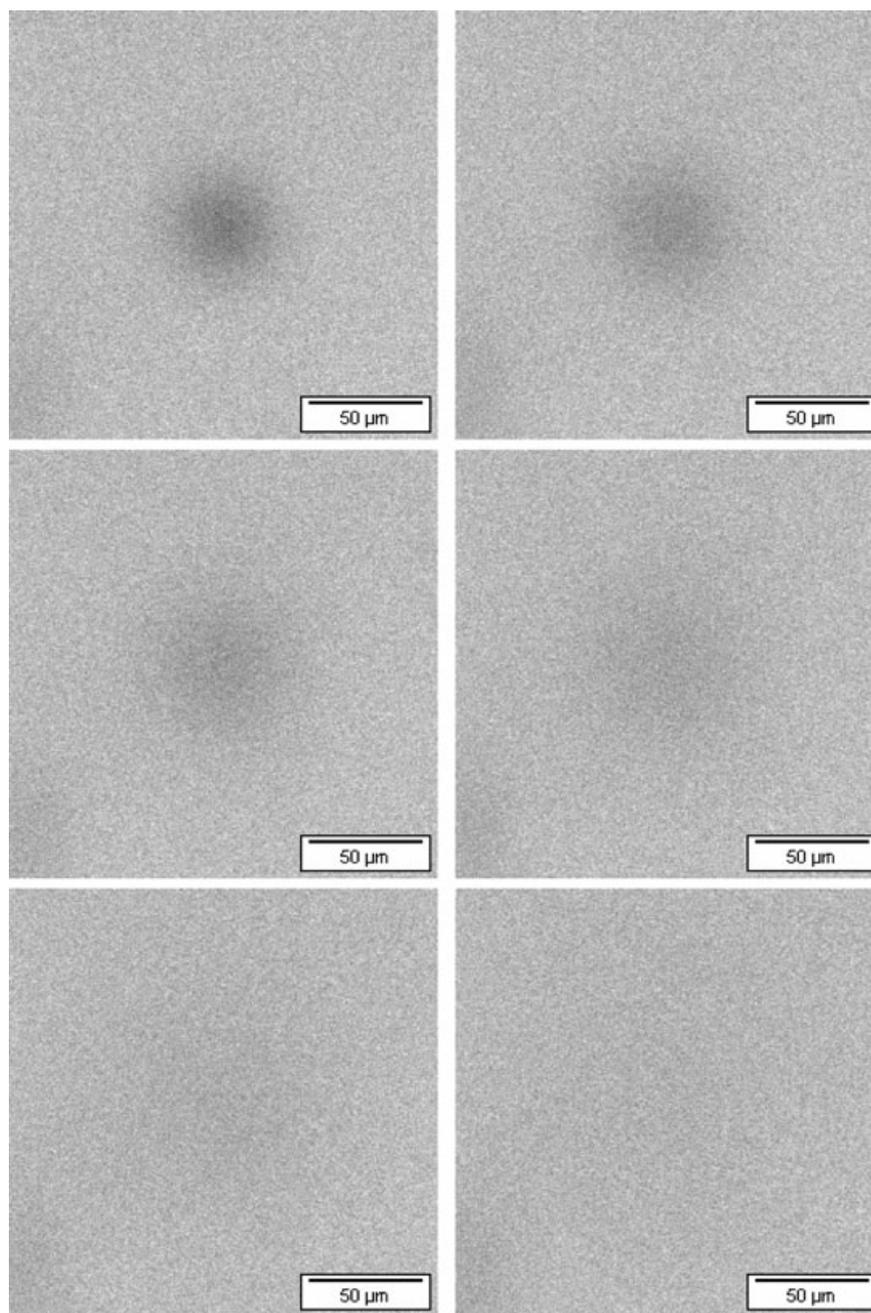
Fig. 2. Plots of original images of the first replicate of the 256×256 images. The first image after bleaching is the one to the left at the top, then follows images about 1 s, 2 s, 4 s, 8 s and 16 s later.

The initial concentration function may be modelled either as an inverse top hat distribution modified by diffusion during a suitable small time interval, or more generally by an arbitrary nondecreasing function in the first image. Both these models are currently being developed, and it turns out that they give more accurate diffusion coefficient estimates at the price of a considerable increase of computation time. The fast Gaussian profile algorithm described in the present paper is sometimes adequate and gives otherwise excellent starting values for the more time consuming methods. It is further possible to consider the scanning of the image by assigning an individual time to each pixel. We can also extend the analysis to irregularly bleached regions and inhomogeneous media, if microscope images are obtained simultaneously with the FRAP measurements. In studies of heterogeneous media we expect that experiments could preferably be performed with many very thin cylindrical bleaching pulses distributed over the volume of interest. Then the Gaussian profile algorithm, being exact for infinitely thin cylindrical pulses, should be highly suitable.
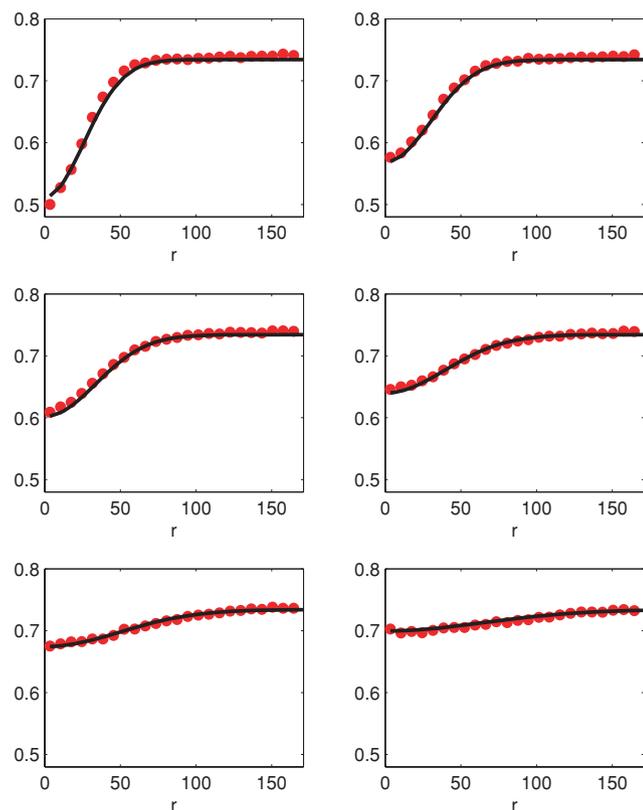
Fig. 3. Plots of the fitted concentration, Eq. (5), and average pixel values for the first replicate of the 256×256 images. The first image after bleaching is the one to the left at the top, then follows images about 1 s, 2 s, 4 s, 8 s and 16 s later.

For optimal design of FRAP experiments we need to find suitable combinations of pixel size, the number of pixels, the number of images in each series, the number of replicates and the number of bleached images in each replicate. The key to optimal design is to find components of variance for each source of variability, and the likelihood approach allows estimation of these variance components. Two such variance components can be obtained from the standard deviations s and s_{repl} in Table 2.

List of symbols

a_0	parameter in the initial concentration function
a_1	parameter in the initial concentration function
C	concentration of unbleached fluorochromes
C_0	initial concentration function
p	pixel value
r_0	parameter in the initial concentration function
r_i	distance of pixel i from the centre of the bleached region
r_r	resolution
σ^2	variance of pixel value
S	set of pixels
T	set of times

References

Alvarez-Mancenido, F., Braeckmans, K., Smedt, S.D., Demeester, J., Landin, M. & Martinez-Pacheco, R. (2006) Characterization of diffusion of macromolecules in konjac glucomannan solutions and gels by fluorescence recovery after photobleaching technique. *Int. J. Pharm.* **316**, 37–46.

Axelrod, D., Koppel, D.E., Schlessinger, J., Elson, E. & Webb, W.W. (1976) Mobility measurements by analysis of fluorescence photobleaching recovery kinetics. *Biophys. J.* **16**, 1055–1069.

Berk, D., Yuan, F., Leunig, M. & Jain, R. (1993) Fluorescence photobleaching with spatial Fourier analysis. Measurement of diffusion in light-scattering media. *Biophys. J.* **65**, 2428–2436.

Blonk, J.C.G., Don, A., van Aalst, H. & Birmingham, J.J. (1993) Fluorescence photobleaching recovery in the confocal scanning light microscope. *J. Microsc.* **169**(3), 363–374.

Braeckmans, K., Peeters, L., Sanders, N.N., Smedt, S.C.D. & Demeester, J. (2003) Three-dimensional fluorescence recovery after photobleaching with the confocal scanning laser microscope. *Biophys. J.* **85**, 2240–2252.

Braeckmans, K., Remaut, K., Vandenbroucke, R.E., Lucas, B., Smedt, S.C.D. & Demeester, J. (2007) Line FRAP with the confocal laser scanning microscope for diffusion measurements in small regions of 3-D samples. *Biophys. J.* **92**, 2172–2183.

Braga, J., Desterro, J.M.P. & Carmo-Fonseca, M. (2004) Intracellular macromolecular mobility measured by fluorescence recovery after photobleaching with confocal laser scanning microscopes. *Mol. Biol. Cell.* **15**, 4749–4760.

Brown, E.B., Wu, E.S., Zipfel, W. & Webb, W. (1999) Measurement of molecular diffusion in solution by multiphoton fluorescence photobleaching recovery. *Biophys. J.* **77**, 2837–2849.

Burke, M.D., Park, J.O., Srinivasarao, M. & Khan, S.A. (2000) Diffusion of macromolecules in polymer solutions and gels: a laser scanning confocal microscopy study. *Macromolecules* **33**, 7500–7507.

Chen, Y., Lagerholm, B.C., Yang, B. & Jacobson, K. (2006) Methods to measure the lateral diffusion of membrane lipids and proteins. *Methods* **39**, 147–153.

Cheng, Y. & Prud'homme, R.K. (2002) Diffusion of mesoscopic probes in aqueous polymer solutions measured by fluorescence recovery after photobleaching. *Macromolecules* **35**, 8111–8121.

Crank, J. (1975) *The Mathematics of Diffusion.* 2nd edn. Clarendon Press, Oxford.

Diaspro, A. (2002) *Confocal and Two-photon Microscopy; Foundations, Applications and Advances*, Chap 5. 1st edn. Wiley-Liss, New York.

Herman, B. (1998) *Fluorescence Microscopy*, Chap. 5. 2nd edn. Bios Scientific Publishers, Oxford.

Hermansson, A.M., Lorén, N. & Nydén, M. (2006) The effect of microstructure on solvent and solute diffusion on the micro and nano length scales. *Water Properties of Food, Pharmaceutical, and Biological Materials*, Chap. 2. 1st edn. CRC Taylor and Francis, Boca Raton.

Keuren, E.V. & Schrof, W. (2003) Fluorescence recovery after two-photon bleaching for the study of dye diffusion in polymer systems. *Macromolecules* **36**, 5002–5007.

Kubitscheck, U., Wedekind, P. & Peters, R. (1994) Lateral diffusion measurements at high spatial resolution by scanning microphotolysis in a confocal microscope. *Biophys. J.* **67**, 948–956.

Kubitscheck, U., Wedekind, P. & Peters, R. (1998) Three-dimensional diffusion measurements by scanning microphotolysis. *J. Microsc.* **192**, 126–138.

Lippincott-Schwartz, J., Snapp, E. & Kenworthy, A. (2001) Studying protein dynamics in living cells. *Nat. Rev. Mol. Cell Biol.* **2**, 444–456.

Lorén, N., Hagslätt, H., Nydén, M. & Hermansson, A.M. (2005) Water mobility in heterogeneous emulsions determined by a new combination of confocal laser scanning microscopy, image analysis, nuclear magnetic resonance diffusometry, and finite element method simulation. *J. Chem. Phys.* **122**, 024716.

Meyvis, T.K.L., Smedt, S.C.D., Oostveldt, P.V. & Demeester, J. (1999) Fluorescence recovery after photobleaching: a versatile tool for mobility and interaction measurements in pharmaceutical research. *Pharmaceut. Res.* **16**(8), 1153–1162.

Pawitan, Y. (2001) *In All Likelihood: Statistical Modelling and Inference Using Likelihood*. Oxford University Press, Oxford.

Pawley, J. (2006) *Handbook of Biological Confocal Microscopy*, Chap. 1. 3rd edn. Springer, New York.

Perry, P.A., Fitzgerald, M.A. & Gilbert, R.G. (2006) Fluorescence recovery after photobleaching as a probe of diffusion in starch systems. *Biomacromolecules* **7**, 521–530.

Phair, R.D. & Misteli, T. (2001) Kinetic modelling approaches to *in vivo* imaging. *Nat. Rev. Mol. Cell Biol.* **2**, 898–907.

Seiffert, S. & Oppermann, W. (2005) Systematic evaluation of frap experiments performed in a confocal laser scanning microscope. *J. Microsc.* **220**, 20–30.

Siggia, E.D., Lippincott-Schwartz, J. & Bekiranov, S. (2000) Diffusion in inhomogeneous media: theory and simulations applied to whole cell photobleach recovery. *Biophys. J.* **79**, 1761–1770.

Smedt, S.C.D., Meyvis, T.K.L., Demeester, J., Oostveldt, P.V., Blonk, J.C.G. & Hennink, W.E. (1997) Diffusion of macromolecules in dextran methacrylate solutions and gels as studied by confocal scanning laser microscopy. *Macromolecules* **30**, 4863–4870.

Sonesson, A.W., Callisen, T.H., Brismar, H. & Elofsson, U.M. (2005) Lipase surface diffusion studied by fluorescence recovery after photobleaching. *Langmuir* **21**, 11949–11956.

Soumpasis, D.M. (1983) Theoretical analysis of fluorescence photobleaching recovery experiments. *Biophys. J.* **41**, 95–97.

Sprague, B. & McNally, J. (2005) FRAP analysis of binding: proper and fitting. *Trends Cell Biol.* **15**, 84–91.

Tsay, T. & Jacobson, K.A. (1991) Spatial Fourier analysis of video photobleaching measurements. Principles and optimisation. *Biophys. J.* **60**, 360–368.

van Oostveldt, P. & Bauwens, S. (1990) Quantitative fluorescence in confocal microscopy: the effect of the detection pinhole aperature on the re-absorption and inner filter phenomena. *J. Microsc.* **158**, 121–132.

Verkman, A.S. (2003) Diffusion in cells measured by fluorescence recovery after photobleaching. *Biophotonics, Part A Methods in Enzymology*. Academic Press, San Diego.

Walther, B., Lorén, N., Nydén, M. & Hermansson, A.M. (2006) Influence of κ-carrageenan gel structures on the diffusion of probe molecules determined by transmission electron microscopy and NMR diffusometry. *Langmuir* **22**, 8221–8228.

Wedekind, P., Kubitscheck, U., Heinrich, O. & Peters, R. (1996) Line-scanning microphotolysis for diffraction-limited measurements of lateral diffusion. *Biophys. J.* **71**, 1621–1632.

Wedekind, P., Kubitscheck, U. & Peters, R. (1994) Scanning microphotolysis: a new photobleaching technique based on fast intensity modulation of a scanned laser beam and confocal imaging. *J. Microsc.* **176**, 23–33.

Weiss, M. (2004) Challenges and artifacts in quantitative photobleaching experiments. *Traffic* **5**, 662–671.

Westrin, B., Axelsson, A. & Zacchi, G. (1994) Diffusion measurements in gels. *J. Contr. Release* **30**, 189–199.